Validation Study for ocean colour product

Annex 1: Evaluation of the aerosol product in the frame of the MERIS atmospheric correction over water

Title	Annex 1: Evaluation of the aerosol product in the frame of the MERIS atmospheric correction over water
Version	1.2
Author(s)	R. SANTER
and affiliation(s)	
	
Modification history	20.12.2008 Final draft
Distribution	

Definitions, Acronyms, Abbreviations

AAOT	
AERONET	Aerosol RObotic NETwork (http://**aeronet**.**gsfc**.**nasa**.gov/)
AOT	Aerosol optical thickness
AU	Astronomic Unit
CalVal	Calibration Validation
ECMWF	European Centre for Medium range Weather Forecasting
ENVISAT	Environmental Satellite
ESA	European Space Agency
GS	Ground Segment
IOP	Inherent Optical Property
IOPA	IOP of the Aerosols
LUT	Look Up Table
MEGS	
MERIS	Medium Resolution Imaging Spectrometer (ESA Envisat)
MERMAID	
MOBY	Marine Optical Buoy
MODIS	Moderate-Resolution Imaging Spectroradiometer (NASA EOS)
NIR	Near Infrared (spectral region)
POLDER	Polarization and Directionality of the Earth's Reflectances (CNES, ADEOS)
RTC	Radiative Transfer Code
SAM	Standard aerosol models
SeaWiFS	Sea-Viewing Wide Field-of-View Sensor (USA)
TOA	Top Of the Atmosphere

1. Introduction

The quality of the MERIS level 1 TOA radiances over the dark ocean in the NIR is a key issue because it ensures the quality of the aerosol retrieval and consequently of the atmospheric correction (Wang and Gordon, 2002). The first requirement brings on the spectral calibration, which allows an accurate knowledge of the Rayleigh scattering. The different approaches to conduct the in flight spectral calibration indicates that an absolute accuracy of 0.1 nm is reached on the determination of the central wavelength (Delwart et al,2007). The second requirement brings on the radiometric calibration, which is realized on board on a reference panel (Delwart et al,2003). The absolute radiometric calibration is assumed to be better that two percent. Vicarious calibration over land targets do not infirm this performance (Schaepman et al,2004). A good inter-band calibration allows selecting the aerosol type. The good absolute calibration is needed to determine the aerosol optical thickness (AOT) but also to select the aerosol model.

Actually, the level 1 radiance is not the starting point of the atmospheric correction. The atmospheric correction is applied on a reflectance corrected from the smile effect, the gaseous absorption and from the sunglint. We detail in the introduction the different steps needed to obtain this reflectance . In addition, we briefly describe the level 2 algorithm and the associated products.

In section 2, we present the data base which combines AERONET and MERIS level 1 and level 2 data. Thanks to MEGS, break points can be added in this data base. We report the comparison on the aerosol product between MERIS and AERONET.

Section 3 is an analysis of the aerosol product

In section 4, we will give recommendation for a next MERIS reprocessing.

1.1. The TOA reflectance over dark water

Conversion radiance reflectance

The level 1B satellite radiance L (w/m^2/µm/sr) is converted into reflectance with:

$$\rho^* = \frac{\pi . L_{1B}}{\mu_s E_S^J} \qquad (1)$$

Where E_S^J is the solar irradiances corrected form the Earth-Sun distance (in UA) at the Julian day J and μ_s the cosine of the solar zenith angle.

Correction of the gaseous absorption

Outside of the strong absorption bands (*i.e.*, in the 761.875 *nm* MERIS band for O_2 and 900 *nm* for H_2O), the coupling between scattering and gaseous absorption remains relatively weak. This assumption leads to express the apparent reflectance ρ^* at top of the atmosphere (TOA) as:

$$\rho^* \approx \rho^*_{na} . T_g , \qquad (2)$$

where ρ^*_{na} is the signal ignoring the gaseous absorption and T_g the gaseous transmittance. This formulation applies for the ozone absorption: the stratospheric ozone is above and auxiliary information on the ozone content allows to simply computing T_g. For the water vapour and residual oxygen absorption, the two gases are mixed with the aerosols and an accurate correction first need the amount of water vapour or oxygen (via the surface pressure) and second some information on the relative vertical scale height of the absorbing gas and of the aerosols. One way to combine the two requirements was suggested by Santer et al, 1999, through a direct link between the residual gaseous absorption in a given spectral band and the band use to determine this gas. For example, the correction of the water vapour at 708 nm is directly related to the 900 nm/885 nm ratio.

The smile effect

For each spectral band, the wavelength varies within the field of view. The in-flight radiometric calibration is based on a standard reflectance panel. Therefore the conversion radiance to reflectance of equation (1) accounts for the so-called smile effect. In the NIR, the residual water

absorption at 708 nm (B9) or the residual oxygen absorption at 778 nm (B12) is not dependent on the smile effect. Equation (2) is no smile effect dependent in the NIR. After conversion in TOA reflectance, the smile effect is accounted for: for each pixel, knowing the central wavelength for each band, a spectral interpolation is done to provide a TOA reflectance at the nominal central wavelengths.

At the end, ρ_{na}^{*} correspond to a MERIS instrument with no smile effect and no gaseous absorption.

The dark water

We limit the wind speed to 7 m/s in order to neglect the contribution of the foam reflectance. The direct sunglint is flagged. For low sunglint, a glint correction is performed. The Cox and Muk (1954) model is used associated to the wind speed available in the auxiliary file and to the direct to direct attenuation computes for a pure molecular atmosphere. The glint correction of ρ_{na}^{*} gives ρ_{ng}^{*}.

ρ_{ng}^{*} is assumed to be to equal the *atmospheric* reflectance ρ_{atm}. ρ_{atm} includes the coupling between the Fresnel reflection and the atmospheric scattering.

1.2. The aerosol reflectance from MERIS

Definition

The aerosol path radiance is defined as:

$$\rho_{aer}=\rho_{ng}^{*}-\rho_{Ray}\,, \qquad (3)$$

The Rayleigh path radiance is computed using the SOS vector code (Deuzé et al, 1989; Lenoble et al, 2007). The inputs to the RTC code are:

(i) The geometrical conditions.

(ii) The barometric pressure for the Rayleigh scattering.

(iii) The wind speed to include a coupling term between Rayleigh scattering and Fresnel reflection on a rough ocean.

Computation

The radiative properties of the aerosols can be computed assuming that the microphysical properties of the particles are well known. The aerosol models correspond to mixtures of aerosol modes characterized by a size distribution and a refractive index. For each of these modes, the particles are generally assumed to be spherical and their inherent optical properties (IOP's) can then be calculated with the *Mie*'s theory. The optical properties of an aerosol assemblage are generated in regards to the percentage of the different components in the mixing.

The aerosol vertical distribution

Three aerosol homogeneous layer are considered:

(i) The stratospheric layer is located between 12 km and 20 km. The standard H2SO4_H2O model is assumed with an AOT at 550 nm of 0.005.

(ii) The upper tropospheric layer is located between 2 km and 12 km. The standard continental model is assumed with an AOT at 550 nm of 0.025.

(iii) The lower tropospheric layer is located between 0 km and 2 km. The aerosol model is retrieved in the NIR

The tropospheric aerosol models

The reference to standard aerosol models (SAM's) is the key element in the interpretation of the Earth's Observation (EO). Because EO generally offers two kinds of information on the aerosols (*i.e.*, the aerosol type and its associated optical thickness), it is therefore mandatory to rely on a family of SAM's such as the models of *Shettle and Fenn* (1979) extensively used for the atmospheric corrections over ocean (*Gordon and Wang*, 1994; *Antoine and Morel*, 1999). These initial SAM's can be adjusted and or complemented by other models to account for specific aerosols such as the absorbing aerosols (*Nobileau and Antoine*, 2005) or the so-called blue aerosols.

1.3. The aerosol remote sensing

The principle (Antoine and Morel, 1999) is to rely on the look-up tables, which allows :

- To calculate the values of $\tau_a(865)$ from the $\rho_{atm}(865)/\rho R(865)$ ratio, for the SAMs.,
- To extrapolate τ_a from 865 to 775 nm, for each aerosol model,
- To obtain the ratios $\rho_{atm}(865)/\rho R(865)$ from τ_a (775), for each aerosol model. These ratios computed from aerosol model, will be noted $\zeta(\lambda)$ in the following.
- To select a couple of aerosol models, by comparing the actual (ρpath(775) / ρR(775)) ratio, and the various $\zeta(775)$ ratios as obtained at the previous step.

1.4. The aerosol product

The Angstroem coefficient α describes the spectral dependence of the AOTs, τ. The dynamic Angstroem coefficient is defined as:

$$\alpha = \ln(\tau_\lambda / \tau_{\lambda'}) / \ln(\lambda / \lambda') \qquad (4)$$

Between 708 and 865, α= -0.16 for the stratospheric aerosols and -1.69 for the continental aerosol

	0.1	0.2	0.5	model
mar_90	-0.36	-0.27	-0.22	-0.17
coa_50	-0.81	-0.76	-0.73	-0.70
rur_99	-1.31	-1.32	-1.32	-1.32

Table 1: Angstroem coefficient, between 708 nm and 865 nm, computed for the 3-layer atmosphere. The AOT of the lower troposphere are 0.1, 0.2, and 0.5. Last column reports for the lower tropospheric model alone.

Last column of Table 1 gives α for 3 tropospheric models: maritime90, coastal50 and rural99. When mixing with the other 2 layers, α depends upon the AOT of the lower layer. Table 1 reports α for three values of the AOT at 550 nm.

2 The MERIS DQWG data base

2.1 AERONET

The standard level-2 aerosol products can be validated using the ground-based measurements of the solar extinction, and the AERONET (AErosol RObotic NETwork) is widely used in this exercise (*Holben et al.*, 1998; *Myre et al.*, 2004).

The CIMEL E-318 is a portable tracking sun-photometer designed to conduct atmospheric studies, and particularly to determine the aerosol optical properties. The latter is equipped of four standard filters: 1020 *nm*, 870 *nm*, 675 *nm* and 440 *nm*. Thanks to two collimators (*i.e.*, *sun* and *sky*) located between the wheel of filter and the electronic box, this instrument offers three scanning protocols: (*a*) *sun*, (*b*) *alm*, and (*c*) *ppl*. For the *sun* mode, the CIMEL selects the *sun* collimator and aims at the sun for measuring the light extinction in each of the four filters. The AOT's at 440 *nm*, 675 *nm* and 870 *nm* are then derived from these measurements.

For a given site, it is possible to automatically download the full archive. We use the AAOT in Venice and Lanai to be coupled to MOBY. AERONET in Villefranche sur mer is located too far from Boussolle and can be not considered.

2.2 MERIS

2.1.1 Extraction protocol

We use the MERIS extraction of the MERMAID database for MOBY in order to rely on the darkness of the water in the NIR (AAOT does not fully fulfil this requirement). We also want to use AERONET data that the reason why BOUSSOLE is not used. Data extraction follows the protocol described in Mazeran, 2007.

2.1.2 The relevant data base with the MEGS break points

We follow the structure of the exel file of the DQWG data base. Yellow is derived from level 1, blue is level 2, green is a break point of MEGS and/or can be produced by a dedicated piece of software, red is additional pieces of information provide by in situ measurement.

The first block informs on the site and on the condition of MERIS overpass. The difference between the CIMEL measurement will be added.

Site	PI	date	time	diff_time	latInSitu	lonInSitu	latSat	lonSat
AAOT	Giuseppe Zibordi	20020620	9.305		45.314	12.508	45.32	12.504

The second block informs on the geometrical conditions and gives the auxiliary meteorological parameters. The scattering angle, given by:

$$\cos(\Theta) = -\cos(SZA)*\cos(VZA) - \sin(SZA)*\sin(VZA)*\cos(dphi)$$

can be computed afterwards in the exel file

thetas	thetav	dphi	scatt_angle	detector	wind	pressure	ozone	humidity	wvap
31.699	36.937	23.861	165.658	898	3.367	1017.734	331.588	49.423	3.137

The third block informs on the aerosol model. Tau and alpha are the regular level 2 product. The information on the two boundary aerosol models and the corresponding mixing ratio are useful to go deeper in the level 2 algorithm.

Tau	alpha	iaer1	iaer2	aer_mix	tau_cimel	alpha_cimel

1.61E-01 1.49E+00 NaN NaN NaN

In this third block, we propose to add the AOT_865 nm and alpha as derived from the CIMEL extinction measurements.

The flags of the fourth block are used for pixel selection.

LAND	CLOUD	ICE_HAZE	HIGH_GLINT	MEDIUM_GLINT	PCD_1_13	PCD_19	OADB	CASE2_S
NaN	NaN	NaN	NaN	NaN	NaN	NaN	NaN	NaN

The fifth bock gives the TOA MERIS signal in the 15 spectral bands.

Toar_412	toar_443	toar_490
9.73E+01	8.57E+01	6.56E+01

to which it is useful to convert the radiance into reflectance:

rhotoa_412	rhotoa_443	rhotoa_490
2.17E-01	1.75E-01	1.30E-01

Or even better in TOA reflectance corrected from the gaseous absorption (and to some extend from the glint).

rho_gc_412	rho_gc_443	rho_gc_490
2.16E-01	1.75E-01	1.31E-01

The transformation of radiance into reflectance requires break points of MEGS.

rho_ray_412	rho_ray_443	rho_ray_490
1.74E-01	1.33E-01	8.86E-02

It is useful to add the Rayleigh reflectance. It is a breakpoint of MEGS.

It is useful as well to have the aerosol reflectance. It is a breakpoint of MEGS.

rho_aer_412	rho_aer_443
2.94E-02	3.11E-02

2.3 Validation of the aerosol product

Tables 2 and 3 reports the match ups respectively for MOBY and AAOT. Figure 1 access the fairly good quality of the retrieval of the MERIS product in AAOT. In B13, MERIS slightly overestimates the AOTs but in B2 the agreement is acceptable. For MOBY, The validation of the AOT_865, reported in figure 2, is poor. The knowledge of the aerosol phase function is a requirement, which is difficult to reach in the backscattering region. Most (2/3) of the MERIS data correspond to this geometry which may explain the poor comparison.

					MERIS		CIMEL	
date	time	thetas	thetav	scatt	tau	alpha	tau	alpha
20020612	20.342	29.7	39.1	164.8	0.076	0.615	0.043	-0.210
20020615	20.437	28.6	30.4	168.9	0.069	0.681	0.040	0.310
20020618	20.532	27.4	20.3	168.4	0.145	0.097	0.025	0.040
20020621	20.626	26.3	9.0	161.7	0.346	0.229	0.043	0.570
20020726	20.626	27.6	9.0	161.0	0.265	0.075	0.033	0.030
20021206	20.956	47.8	30.1	110.0	0.025	0.516	0.032	0.200
20021210	20.531	51.3	20.4	141.0	0.088	0.295	0.063	-0.190
20021213	20.625	51.0	9.0	135.0	0.05	0.174	0.034	-0.360
20021219	20.813	50.2	14.4	119.4	0.22	0.075	0.034	-0.110
20021222	20.908	49.7	25.1	111.6	0.063	0.571	0.036	0.840
20021226	20.483	53.0	25.6	142.6	0.025	0.648	0.012	0.230
20030113	21.049	48.2	38.6	101.2	0.031	1.552	0.043	1.330
20030202	20.578	48.9	14.9	142.4	0.044	0.163	0.030	-0.190
20030212	20.341	49.1	39.2	156.8	0.069	0.593	0.026	-0.330
20030426	20.437	29.6	30.4	178.6	0.094	0.35	0.064	0.060
20030429	20.531	27.9	20.3	172.3	0.057	0.659	0.067	0.350
20030502	20.626	26.2	9.0	162.7	0.057	0.935	0.112	1.010
20030512	20.388	28.8	35.0	171.4	0.057	0.736	0.035	0.760
20030515	20.483	27.3	25.6	174.0	0.202	0.218	0.037	0.320
20030521	20.672	24.6	3.1	158.4	0.391	0.075	0.069	0.070
20030721	20.391	30.8	35.0	170.1	0.258	0.339	0.070	-0.200
20030809	20.439	30.7	30.5	176.2	0.101	0.417	0.049	-0.330
20030812	20.533	29.5	20.4	170.6	0.164	0.328	0.047	-0.360
20030815	20.628	28.4	9.1	160.7	0.271	0.097	0.049	0.370
20030828	20.487	31.1	25.6	174.0	0.025	0.681	0.011	-0.760
20030916	20.534	32.7	20.4	165.3	0.094	0.439	0.028	0.510
20030919	20.628	32.1	9.0	156.1	0.082	0.218	0.026	1.520
20030929	20.391	36.7	35.0	165.4	0.057	0.857	0.004	5.420
20031005	20.58	35.9	14.9	155.8	0.063	0.185	0.005	1.360
20031008	20.675	35.7	3.1	146.9	0.094	0.119	0.003	2.420
20031015	20.344	40.6	39.2	159.2	0.063	0.571	0.009	-1.470
20031021	20.532	40.3	20.4	153.4	0.019	0.075	0.019	0.750
20031024	20.627	40.2	9.0	146.3	0.088	0.670	0.039	1.230
20031105	21.004	40.6	34.5	112.4	0.302	0.075	0.089	0.280
20031106	20.485	44.7	25.6	150.2	0.050	0.560	0.058	0.480
20031118	20.862	44.9	19.9	120.5	0.523	0.075	0.034	0.640
20040131	20.438	50.7	30.4	150.1	0.044	0.494	0.019	0.550
20040203	20.532	49.2	20.3	145.9	0.076	0.494	0.042	0.160

Table 2: MOBY_Lanai: date, time of MERIS overpass, MERIS geometrical conditions , MERIS aerosol product (AOT_865 and $-\alpha$), CIMEL AOT_865 and α(670,870).

					MERIS		CIMEL	
date	time	thetas	thetav	scattering	tau	alpha	tau	alpha
20020813	9.351	38.9	33.7	160.5	0.059	1.49	0.025	2.91
20021201	10.061	68.3	27.3	95.9	0.056	0.72	0.020	1.41
20021202	9.541	70.1	18.8	119.5	0.061	0.70	0.029	1.05
20030105	10.061	69.9	27.3	93.1	0.154	0.28	0.097	0.66
20030207	9.446	66.3	26.7	129.7	0.034	0.79	0.013	0.27
20030209	10.06	62.8	27.3	98.2	0.167	1.13	0.065	0.84
20030225	10.013	57.5	23.6	105.4	0.035	0.78	0.014	0.21
20030314	9.446	54.1	26.7	142.3	0.096	0.94	0.059	1.32
20030323	9.731	48.9	1.5	132.2	0.127	1.09	0.082	0.96
20030418	9.447	41.0	26.6	155.1	0.173	1.43	0.121	1.59
20030926	10.111	48.0	30.8	110.1	0.115	0.65	0.037	1.83
20031010	9.448	55.7	26.6	137.6	0.079	0.78	0.049	2.76
20031025	9.921	58.9	15.8	111.6	0.079	1.17	0.043	0.87
20031104	9.684	62.8	6.1	120.5	0.077	0.99	0.047	1.20
20031110	9.874	63.9	11.6	109.5	0.089	0.65	0.039	1.50
20031113	9.968	64.5	19.7	104.1	0.147	1.53	0.116	2.04
20031129	9.922	68.3	15.7	102.8	0.034	0.48	0.049	1.50
20031209	9.685	70.6	6.0	112.7	0.072	0.08	0.018	0.69
20031216	9.353	72.6	33.8	124.0	0.032	0.08	0.009	0.00
20040101	9.306	73.2	36.9	125.7	0.046	0.82	0.023	1.41
20040927	9.542	51.1	18.9	139.6	0.026	0.46	0.011	2.55
20041209	9.637	70.8	10.3	114.7	0.109	0.51	0.094	1.14
20041215	9.826	70.7	7.3	105.1	0.056	0.89	0.024	0.75
20051013	9.969	54.8	19.8	112.6	0.205	1.62	0.142	2.07
20051118	9.448	67.7	26.6	125.0	0.038	0.45	0.021	0.75

Table 3: same as table2 for AAOT.

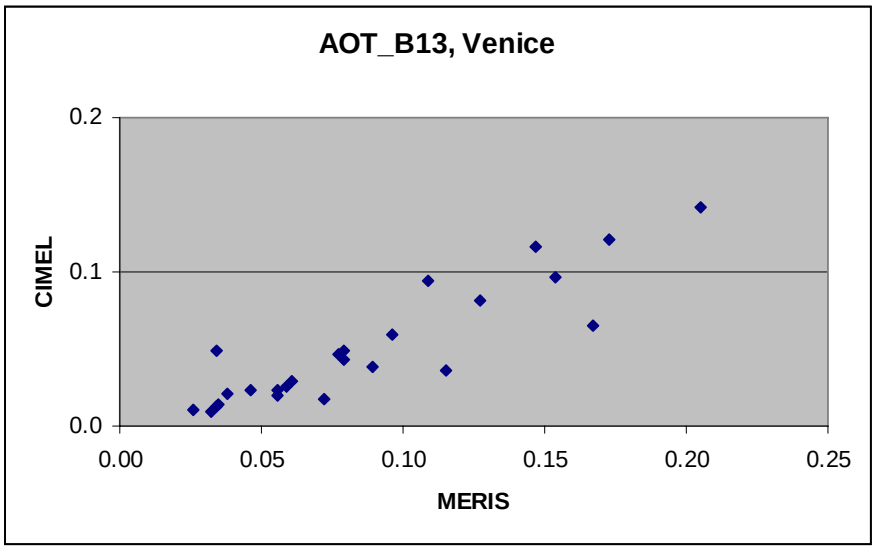

(a)

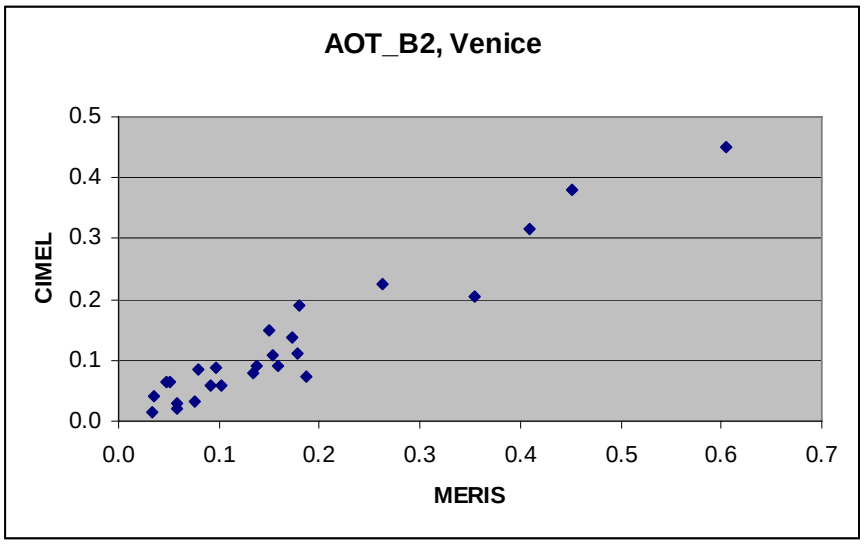

(b)

Figure 1 : AAOT, comparison between MERIS retrieved AOT and CIMEL measured AAOT at 865 nm (B13)(a) and at 442 nm (B2), (b).

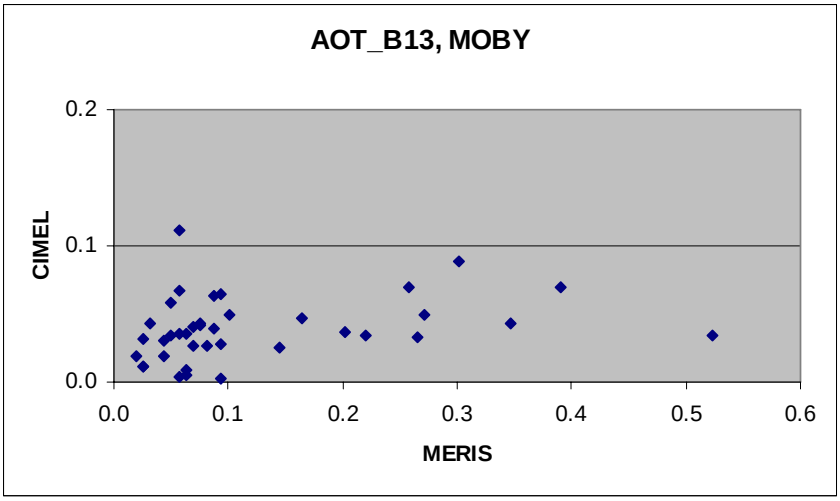

(a)

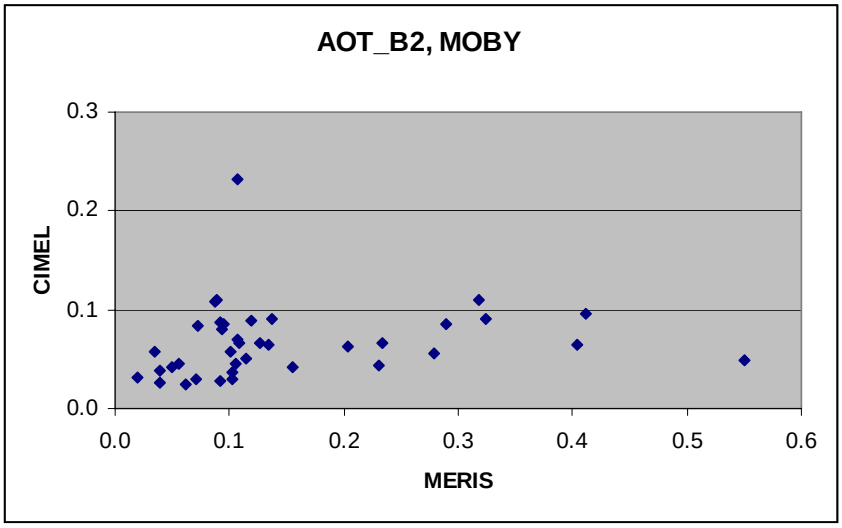

(b)

Figure 2 : MOBY, comparison between MERIS retrieved AOT and CIMEL measured AAOT at 865 nm (B13)(a) and at 442 nm (B2), (b).

2.4 The spatial heterogeneity of the aerosol product

The validation of the aerosol product has been done on a 5 by 5 pixels window. We now investigate the spatial dispersion of the aerosol product within a window. We use the MOBY data set because we believe that the aerosol type is quite homogeneous (few regional sources of the aerosol emission) at least compared to AAOT.

On the data file, we first used the level 1 flags to select our points. None of the following is raised:

LAND	CLOUD	ICE_HAZE	HIGH_GLINT	MEDIUM_GLINT

Then, we counted the number of different pairs of selected aerosol models in the window. We also average the different level physical values to produce in table 3, the mean AOT and it relative dispersion, the mean α and it absolute dispersion.

Figure 3 illustrates the dispersion of the aerosol models through the number of aerosol pairs selected in the window. There is no correlation between the dispersion in α and the number of pairs which is a priori a surprise: you expect to catch more different aerosol models where the spatial dispersion of α is larger.

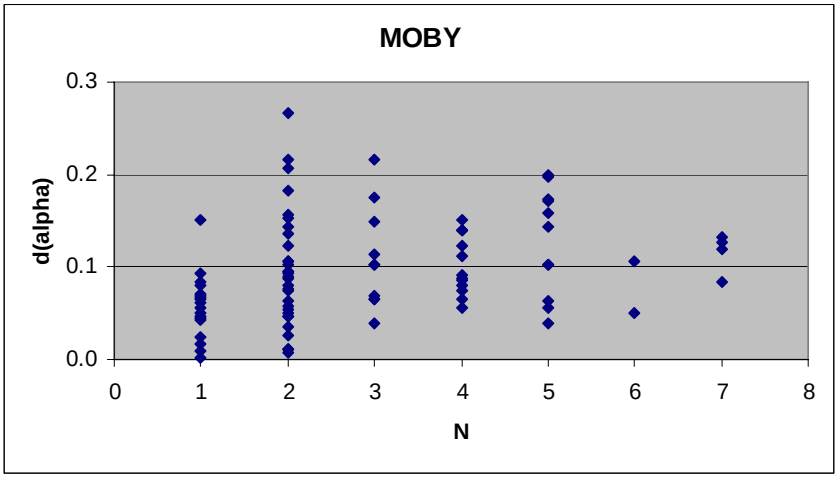

Figure 3: relation between N (number of SAM pairs) and the dispersion of α

2.5 The spectral dependence of the aerosol path radiance

We are now talking about the spectral dependence of the aerosol path radiance with as concern:

(i) The need to assess a spectral dependence in the NIR in the BPAC method.

(ii) The need to validate the behaviour of the TOA signal in B13. Two reasons to that: the stray light correction is an issue as well as the linearity of the SI detector.

One simple criterion is to compare ro_aer measured in B13 to it extrapolated value derived from B9_B12 (Huot, 2008). This extrapolation is a priori done on a log-log scale (ro_are vs lambda). Results are reported in figure 4; A bias of about 3 percent appears and need to be investigated.

date	#	model	tau	dtau	alpha	dalpha	B13_aer	epsilon
20020530	20	4	0.052	0.012	0.70	0.14	22.1	26.4
20020612	25	2	0.077	0.002	0.54	0.09	2.1	15.2
20020615	10	2	0.073	0.010	0.58	0.16	14.5	36.1
20020618	20	2	0.106	0.043	0.34	0.15	39.2	71.0
20020707	18	3	0.153	0.039	0.51	0.15	26.3	27.2
20020720	24	3	0.053	0.051	0.76	0.07	5.9	9.2
20020723	18	2	0.128	0.017	0.38	0.09	13.3	38.1
20020827	25	3	0.099	0.004	0.52	0.07	3.9	13.3
20020912	22	4	0.059	0.004	0.77	4.77	4.3	11.6
20020928	25	3	0.049	0.002	0.67	0.92	2.2	11.9
20020928	19	3	0.168	0.024	0.34	0.95	13.5	14.7
20021001	2	1	0.114	0.000	0.49	0.00	0.0	0.4
20021020	23	2	0.042	0.005	0.28	0.11	7.2	22.3
20021030	10	2	0.029	0.003	0.64	0.10	2.1	8.6
20021121	25	2	0.033	0.002	0.43	0.14	3.9	16.6
20021127	24	5	0.077	0.032	0.67	0.17	27.2	19.7
20021127	19	1	0.086	0.003	0.33	0.05	3.9	10.3
20021127	19	1	0.050	0.004	0.21	0.09	3.0	18.0
20021226	22	2	0.027	0.001	0.50	0.14	5.6	13.4
20030202	17	2	0.046	0.002	0.20	0.10	3.2	22.6
20030202	13	1	0.070	0.002	0.47	0.05	2.4	9.2
20030426	25	1	0.093	0.003	0.31	0.04	1.1	2.9
20030429	25	5	0.060	0.005	0.71	0.06	1.5	8.5
20030512	25	5	0.059	0.002	0.73	0.04	2.5	8.9
20030515	20	3	0.149	0.026	0.47	0.11	17.9	27.1
20030515	9	3	0.227	0.050	0.37	0.10	21.2	82.8
20030809	25	3	0.098	0.003	0.46	0.07	2.6	8.4
20030812	25	2	0.164	0.018	0.29	0.06	11.1	31.7
20030828	25	3	0.027	0.001	0.53	0.17	3.5	17.0
20030916	23	2	0.092	0.004	0.52	0.06	4.7	10.4
20030929	25	6	0.054	0.003	0.84	0.11	5.5	15.2
20031005	9	1	0.069	0.002	0.19	0.07	3.3	30.8
20031015	18	1	0.064	0.003	0.47	0.08	4.2	12.3
20031021	14	3	0.021	0.002	0.31	0.22	9.3	35.5
20031024	15	5	0.071	0.006	0.71	0.06	4.2	6.9
20031106	25	1	0.062	0.008	0.51	0.06	13.5	10.1
20031122	25	2	0.047	0.008	0.36	0.08	14.8	13.9
20031122	15	2	0.031	0.006	0.41	0.21	15.9	30.0
20031211	16	1	0.097	0.006	0.16	0.05	6.5	14.1
20040105	5	1	0.113	0.006	0.10	0.02	5.8	44.0
20040131	5	2	0.045	0.006	0.48	0.01	6.1	6.5
20040203	16	1	0.077	0.004	0.43	0.08	5.3	14.7
20040219	21	2	0.074	0.010	0.66	0.03	2.3	5.3
20040222	21	4	0.062	0.012	0.70	0.12	18.8	14.8
20040312	25	4	0.053	0.004	0.64	0.11	1.8	13.7
20040413	21	5	0.120	0.044	0.53	0.16	30.2	51.3
20040518	8	1	0.082	0.001	0.67	0.01	0.9	2.9
20040705	18	2	0.062	0.179	0.66	0.05	2.6	8.4
20040708	25	2	0.057	0.002	0.66	0.07	3.6	11.9
20040711	25	7	0.073	0.028	0.66	0.13	44.1	20.4
20040711	15	2	0.034	0.001	1.00	0.05	3.0	5.8
20040724	22	7	0.068	0.015	0.67	0.12	19.1	24.6
20040727	25	7	0.034	0.009	0.88	0.13	25.2	21.1
20040831	24	2	0.057	0.025	0.43	0.18	42.1	57.5
20040903	25	2	0.058	0.011	0.25	0.09	16.5	30.3
20040916	25	2	0.083	0.003	0.51	0.05	3.3	9.1
20041122	21	4	0.027	0.021	0.69	0.14	74.7	19.0
20041211	22	1	0.049	0.001	0.19	0.07	2.8	16.2
20041213	25	5	0.037	0.007	0.67	0.10	3.4	7.1
20041214	25	4	0.053	0.003	0.74	0.07	3.0	6.4

Table 3: Selected MODY data: date, number of validated points, number of SAM pairs, level 2 AOT_865, rms of this AOT in the window, level 2 – alpha, rms of this α, relative dispersion (rms/mean in percent) of the aerosol path radiance in B13, relative dispersion (rms/mean in percent) of ε(B12, B13).

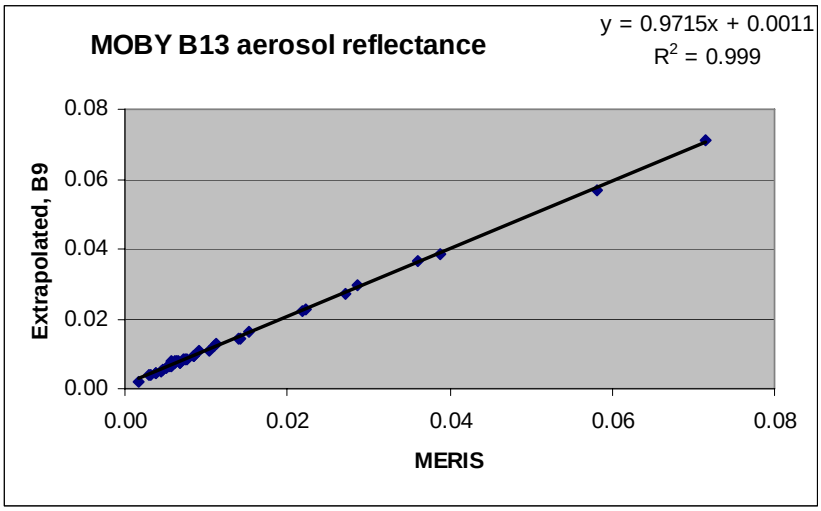

Figure 4: Aerosol reflectance in B13 in MOBY: measured versus extrapolated. Results from a linear regression are displayed.

3. Analyse the aerosol product

3.1 The selection of the aerosol model and the spatial variability

The Gordon coefficient ε describes the spectral dependence of the aerosol reflectance. The dynamic Gordon coefficient is defined as:

$$\varepsilon = \ln(\rho_a^{\lambda}/\rho_a^{\lambda'})/\ln(\lambda\ /\lambda') \quad (5)$$

In a near primary scattering regime, ρ_a^{λ} is proportional to τ_a^{λ}. The proportionality is driven by the aerosol phase function p_a^{λ} and the aerosol single scattering albedo w_a^{λ}. At a given scattering angle, the dependence of $p_a^{\lambda}\ w_a^{\lambda}$ versus ε is discontinuous as indicated in figure 5. Therefore, a small variation in ε can result in a large variation of $p_a^{\lambda}\ w_a^{\lambda}$ mainly in the backscattering region in which the influence of the nature of the aerosol is strong.

The AOT at 865 nm is derived from the measurement of the aerosol reflectance at 865 nm. The discontinuity of the relation $p_a^{\lambda}\ w_a^{\lambda}$ versus ε provokes an amplification of the dispersion of the AOT on a given window as illustrated in figure 6. If an unique aerosol model is used in the 5*5 pixels window, then the plot follows the 1 by 1 line.

Of course, this artificial spatial heterogeneity on the aerosol model should impact on the retrieval of the water leaving radiance.

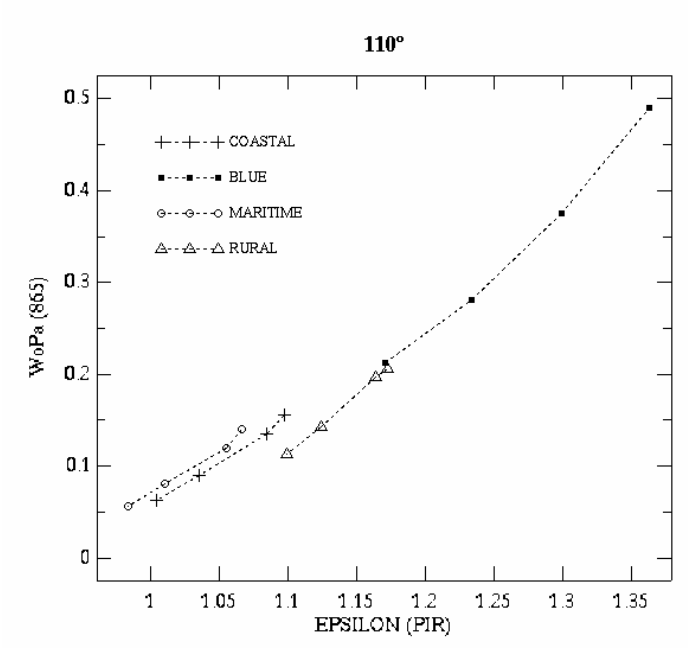

(a)

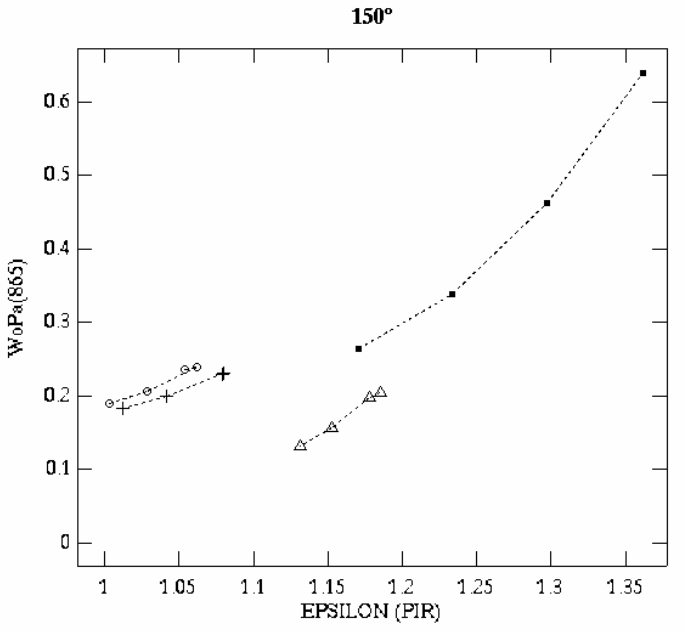

(b)

Figure 5: ε and the selection of the aerosol phase function at a scattering angle of 110° (a) and 150° (b). x axis is the exponential of ε .

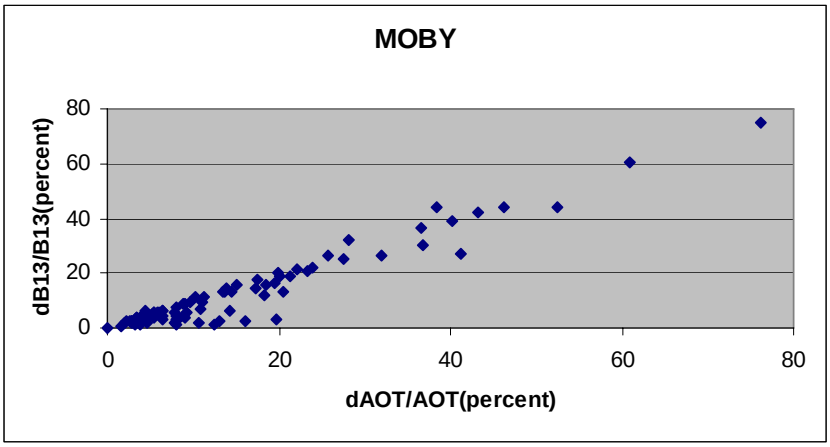

*Figure 6: in the 5*5 pixels window, relative dispersion of the retrieved AOT versus the relative dispersion of the aerosol reflectance in B13*

3.2 The spectral dependence of the aerosol reflectance

We want to analyse the figure 4 results is which in B13 few percent difference exist between the aerosol reflectance extrapolated from B9-B12 and B13. We use the primary scattering approximation to evaluate the ln_ln behaviour of the aerosol reflectance versus the scattering angle Θ. ρ_a^λ is proportional to $\tau_a^\lambda\ p_a^\lambda\ w_a^\lambda$; actually to the sum of the stratospheric contribution, of the upper troposphere and of the mixing layer. Following Eq. (5), we compute ε between B9 and B12. Then we extrapolated in ln-ln to get $\tau_a^\lambda\ p_a^\lambda\ w_a^\lambda$ in B13 and we compared to the computed value for B13. The computation is done in the scattering angle range (90°, 180°). Figure 7 reports the results for the M90 model (Maritime, 90% humidity). The result of the linear regression clearly indicates that the ln-ln law applies. We did the same exercise with the C50 model (Coastal, 50 % humidity) and the slope of the regression is 0.9923 for an offset of 9E-05. The 3 percent bias in figure 4 is not expected.

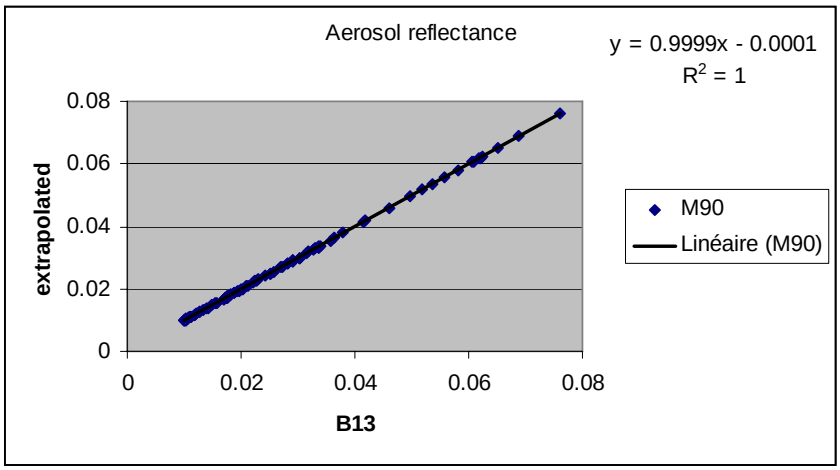

Figure 7: Aerosol reflectance in B13: computed versus extrapolated B9-B12 for the M90 model. Results from a linear regression are displayed.

3.3 The aerosol optical thickness

The extraction of the AOT from the aerosol reflectance requires the knowledge of p_a^λ w_a^λ. For the AAOT, the AERONET climatology in α gives a mean of –1.8 and –0.4 for Lanai, figure 8.

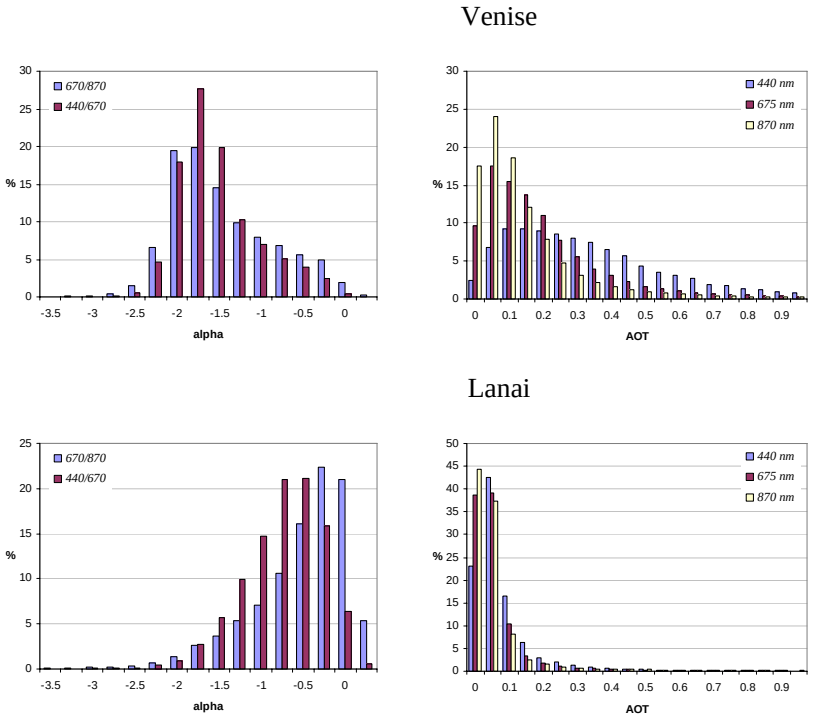

Figure 8:Climatology of the AOTs and associated α from the AERONET stations in Venice and Lanai.

On the other hand, thanks to the IOPA project, we have a climatology of the aerosol phase functions (Zagolski et al, 2007). Figure 9 gives a comparison on the aerosol phase function between the computed values for the standard model and the measured for a common α in the NIR. For Lanai, the tropospheric aerosol model ranges from the M99 to the C50 models. In AAOT, we selected a Junge size distribution implemented in the ground segment to represent the "bleu" aerosols. In the scattering angle range 90°-150°, the theoretical phase function is always under estimated resulting in the observed over estimated MERIS AOT (see figure 1 for AAOT).

It does not explain the MOBY results of figure 2. The MOBY geometrical conditions in the backscattering (see table 2) may explain the poor comparison between MERIS and CIMEL AOT. The phase function in backscattering is not well predictable because of it high sensitivity to the refractive index.

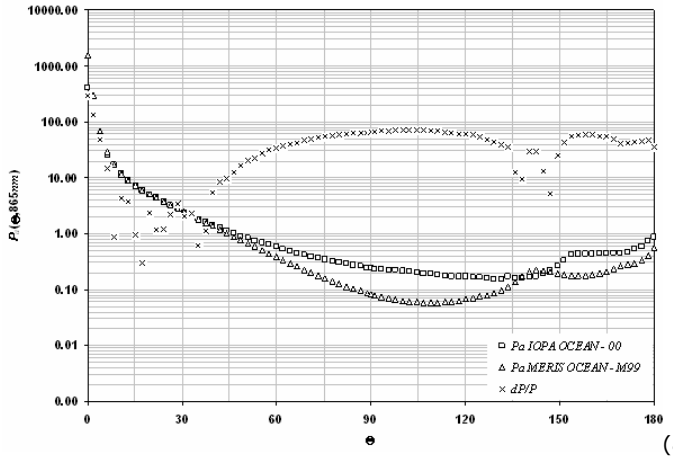

(a)

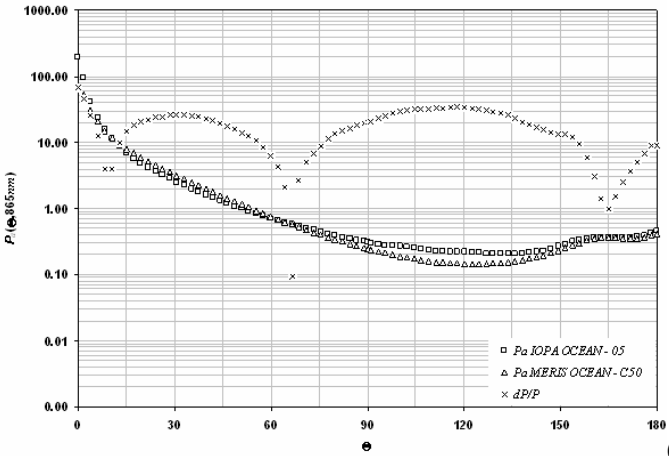

(b)

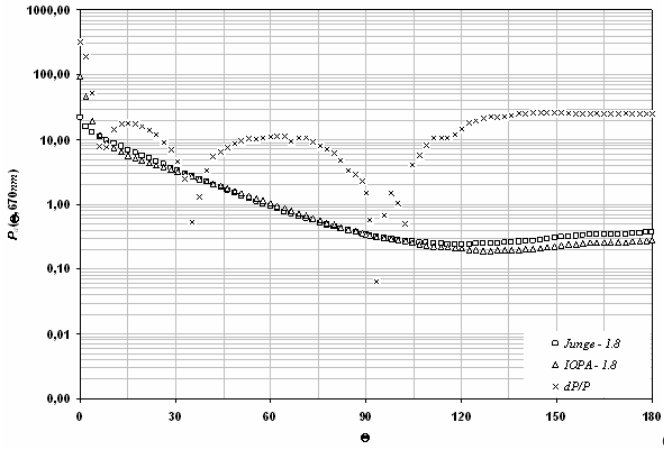

©

Figure 9:Aerosol phase function at 865 nm versus the scattering angle. Comparison between standard model (triangle) and AERONET derived values. Percent difference between the two phase functions is reported as well. The 3 plots correspond to (a) the maritime model for α=0, (b) the coastal model for α=-0.5, (c) the Junge model for α=-1.8.

4. Recommendations

4.1 The selection of the aerosol model

4.1.1 Applying a standard correction for high visibilities

The selection of the aerosol model is based on the retrieval of ε. For high meteorological visibilities, ε is very sensitive to the radiometric calibration. In order to evaluate this effect, we applies a multiplicative factor g to the TOA reflectance. Using Eq. (5), we compute ε versus the scattering angle. This computation assumes the primary scattering regime. Figure 10 reports the results for the M90 aerosol model with two AOTs at 550 nm: 0.05 and 0.1. We considered a two percent error on the absolute radiometric calibration both at 778 nm and 865 nm.

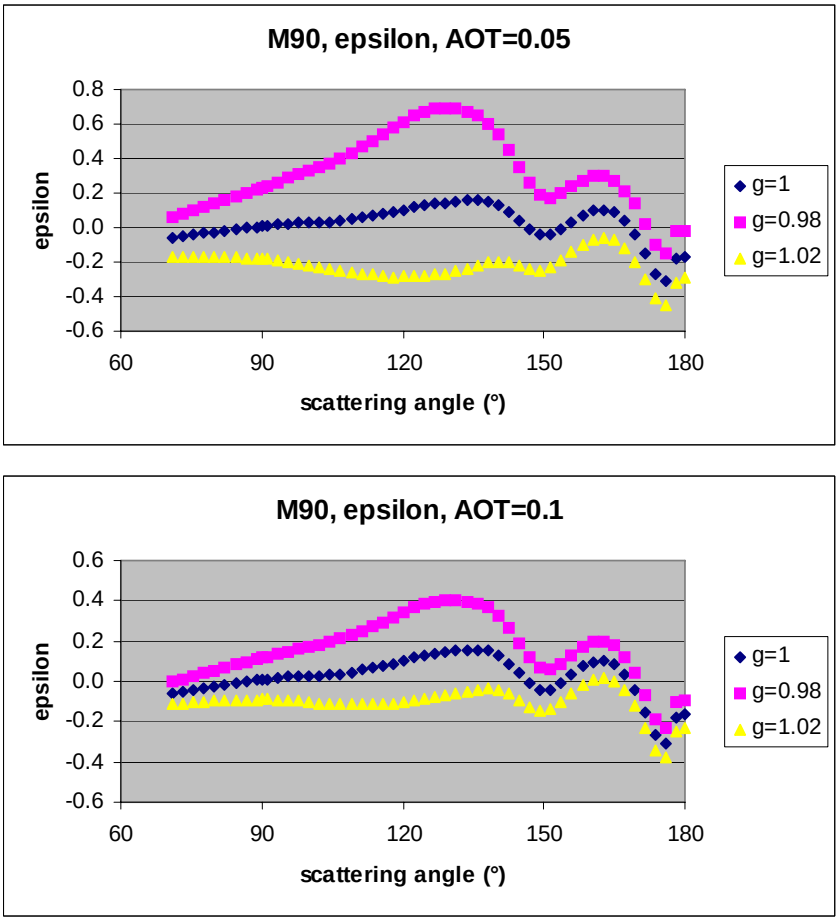

Figure 10: Influence of the radiometric calibration on ε.

The results of figure 10 have to be compared with the sensibility of ε with the aerosol model as reported in figure 11. Schematically, it seems difficult to detect an aerosol type below AOT=0.05 as least better than what an aerosol climatology can predict.

On a practical point of view, let us assumed the M90 model as default model for AOT_550 less than 0.05 (0.047 at 865 nm). For the model M90, based on the primary scattering approximation:

$$\rho_a = \tau_a * P_a / 4\mu_s\mu_v \quad (6)$$

we can compute the aerosol reflectance at 865 NM. Below this threshold, the atmospheric correction will be conducted with the model M90 including the retrieval of the AOT_865 as:

$$AOT\_865 = = 4\mu_s\mu_v(\rho_{ng}^{B13} - \rho_{BG}^{B13}) / P_a^{M90,865} \quad (7)$$

Where ρ_{BG}^{B13} is the signal with no aerosols in the lower troposphere.

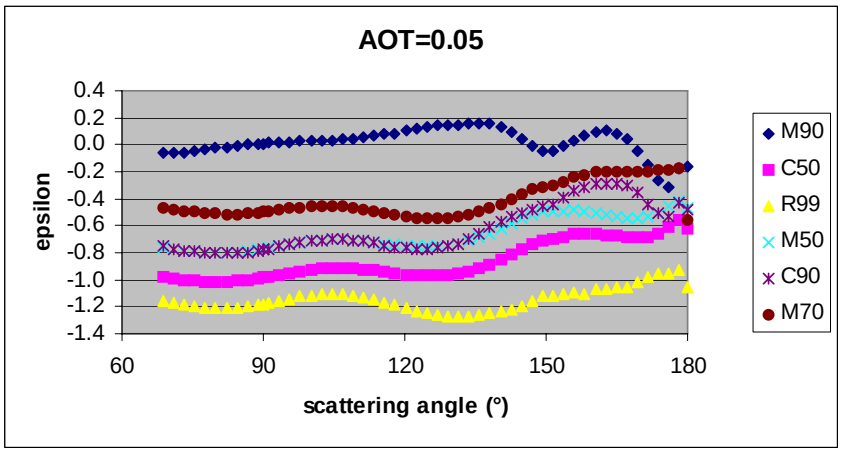

Figure 11: Aerosol model and ε.

4.1.2 Use SAMs with a continuity on the IOPs

We saw in §3.1 and through the figure 5, an induced "noise" on the aerosol product which results in the discontinuity of the inherent optical properties of the aerosols. A simple recommendation is then to use a set of aerosol models which offers a good continuity of the IOPs. It is the case for the Junge models selected for the MERIS aerosol remote sensing over land. It as well true in the real life through the analysis of the AERONET sky radiance measurements conducted in the ESA IOPA project. This continuity is illustrated in figure 12. For a given scattering angle, the aerosol phase function varies continuously with α.

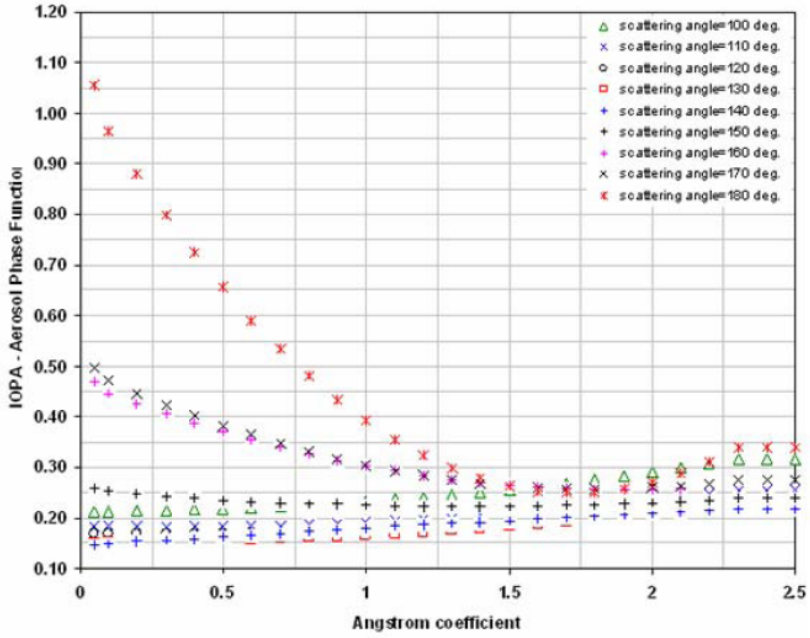

Figure 12: Continuity of the aerosol phase function at 865 nm versus α.

4.1.3 The atmosphere above the mixing layer

Because of the high visibilities encountered in MOBY, it is certainly possible to evaluate the aerosol background distributed in the stratosphere and in the upper troposphere.

AOTs of the stratospheric layer and of the upper troposphere are reported in table 4 in B12 and B13 as well as α.

	B12	B13	alpha
conti	0.0141	0.0118	-1.72
strato	0.0047	0.0047	-0.16
total	0.0188	0.0163	-1.34

Table 4: the back ground upper atmosphere. AOT and α for the two layers and for the total.

To the MOBY MERIS level 2 AOT, we subtract 0.0163. We now plot α, corresponding to the atmospheric column, versus the AOT of the mixing layer in figure 13. If AOT_ML=0 and if the upper atmosphere is well described, then we should have α=-1.34 which is not the case when applying a linear regression. The offset, α=-0.53, suggest a smaller spectral dependence of the upper troposphere than for the standard continental model. The weak slope of the linear regression in figure 13 also suggests that the spectral dependence of the AOTs is quite identical between the ML and above.

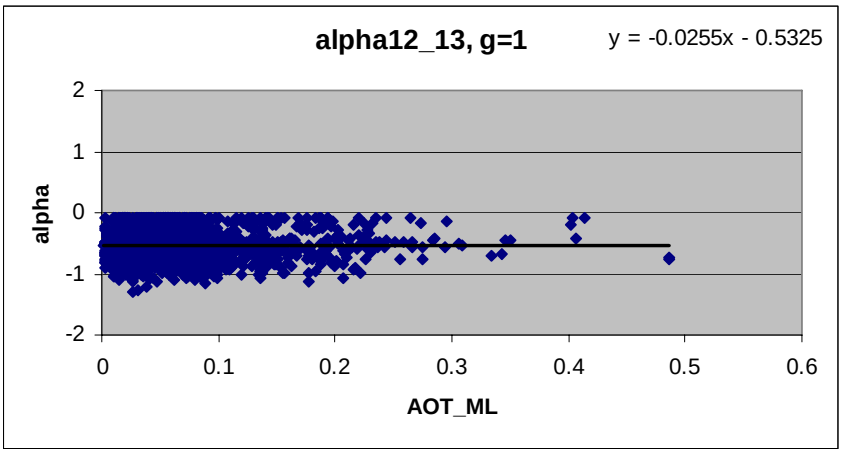

Figure 13: α versus the AOT of the mixing layer

If we consider the climatology of AERONET in Mauna Loa, figure 14, at 3000 m elevation not so far from MOBY, you have in the NIR, α=–0.2 or so. Therefore, the assumed continental model does not reflect the measured spectral dependence of the AOTs… if you believe to be able to get α in mean with quite small AOTs.

Clearly this analysis supports the use of the IOPA models. The retrieval of the aerosol phase functions integrated on the atmospheric column implicitly includes the vertical distribution.

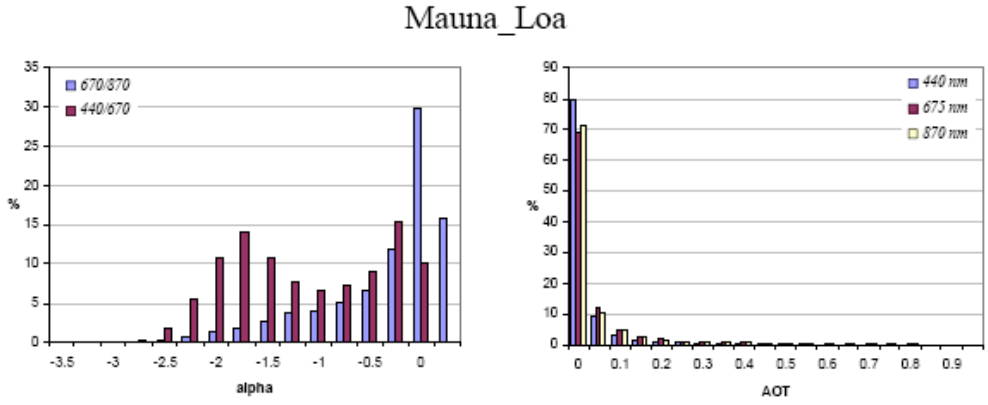

Figure 14: same as figure 8 but at Mauna Loa.

4.2 Absolute calibration of MERIS in the NIR

4.2.1 Using α

We need auxiliary information to validate the MERIS retrieved ε and α. A strong assumption can be considered as an auxiliary information. Assuming a standard aerosol model and *g_865=1*, the so-called vicarious adjustment (Franz et al, 2007) plays this game : *g_778* is set to the value which allows to detect this SAM. This adjustment is dependent of the specific algorithm which is used to remote sense the aerosols.

The best way to go is to directly use ε from MERIS and to play with ground based measurement of ε. We will describe this approach in §4.2.2. Alternatively, we can use α from MERIS and compare to α CIMEL. This comparison is possible thanks to the MERIS level 2.

It is possible to study the impact of the calibration on the MERIS level 2 AOTs: AOT_865 and AOT_778 which is derived from the former and from α. Let us assume that the TOA radiance is multiply by the corrective factor g. It derives from Eq. (6):

$$d\rho_{aer}=(g-1)\rho^{*}_{na}. \qquad (8)$$

At a first approximation:

$$d\tau_{aer}/\tau_{aer} = d\rho_{aer}/\rho_{aer} \qquad (9)$$

At the end, we get the AOT as they should be produced by MERIS from different gains apply on the current radiometric calibration. This exercise directly applies to B13 and B12. It can be applied to B10 and B9 as far as the spectral dependence of the AOT follows a log-log dependence with the wavelength. To make the comparison with CIMEL ($\alpha(670\_870)$), we selected B9 and B13. Figure 15 is a comparison for MOBY_Lanai between MERIS and CIMEL. This comparison is done for 4 gains equally apply to all the MERIS bands. The α values are quite scattered but clearly we can exclude gains above 1.01 (g=1.05 is out of range) and below 0.99.

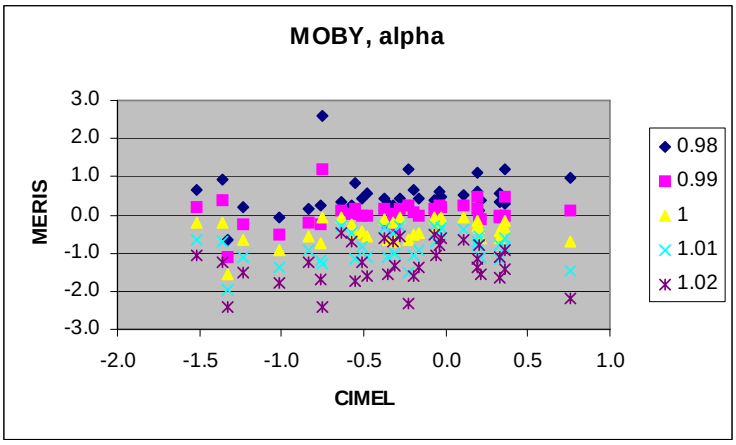

Figure 15: α MERIS computes for 4 gains versus α CIMEL

Even, if this approach relies on the MERIS AOT_865, the result should be not dependant upon the algorithm because if the AOT_865 is bias, it is the same bias on the AOT_778 and therefore it should not have any impact on α.

Figure 15 is difficult to interpret because the results are scattered. To reduce the errors, table 5 gives the mean value. *g=1* is perfect. Back to the CIMEL climatology of figure 8, *g=1.0* is also a good candidate. Let say that MERIS is well calibrated at better than 1 percent.

gain	CIMEL	0.98	0.99	1.00	1.01	1.02
alpha	-0.14	0.42	0.00	-0.41	-0.82	-1.21

Table 5: mean value of α from figure 15

The comparison between MERIS is a trade off:

(i) The sensitivity of α (or ε) to the radiometric calibration is the highest for a low aerosol loading.

(ii) Conversely, the accuracy of α from the CIMEL AOTs is poor for a low aerosol loading.

A simple error analysis on the CIMEL AOT is based on:

(i) A relative error E on the radiometer calibration in irradiance results in an absolute error on the total optical thickness (or to the AOT) of:

$$d\tau_{aer}=E/\mu_s \qquad (10)$$

(ii) It results in an error in α:

$$d\alpha(\lambda_1,\lambda_2)=(1/\ln(\lambda_1/\lambda_2))(d\tau^1_{aer}/\tau^1_{aer}-d\tau^2_{aer}/\tau^1_{2aer}) \qquad (11)$$

For a CIMEL at 670 nm and 870 nm, we assume than E_2=0.01 and than E_2=0.005. It corresponds to an absolute calibration achieved at 1 percent (which is realistic using a Langley Bougueur plot calibration) and to an interband calibration better than 0.5 percent. Figure 16 gives the resulting error on the CIMEL measurements at Lanai.

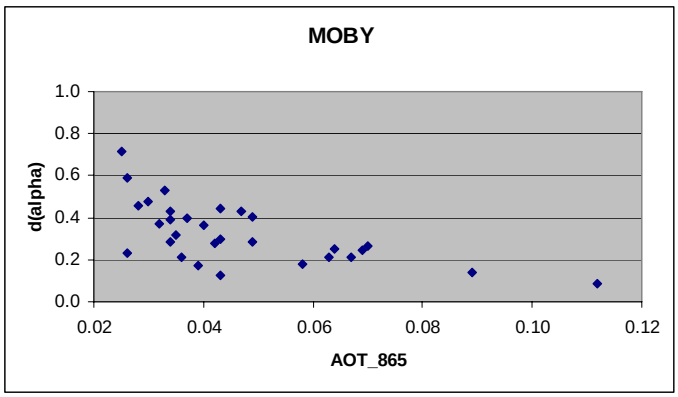

Figure 16:Error on α CIMEL on the MOBY data set.

AOTs below 0.04 can not provide reliable values and are excluded in figure 17. An upper threshold of 0.12 on the AOT is also applied because above that, α from MERIS in no longer sensitive to the radiometric calibration. Above results on the calibration are still valid.

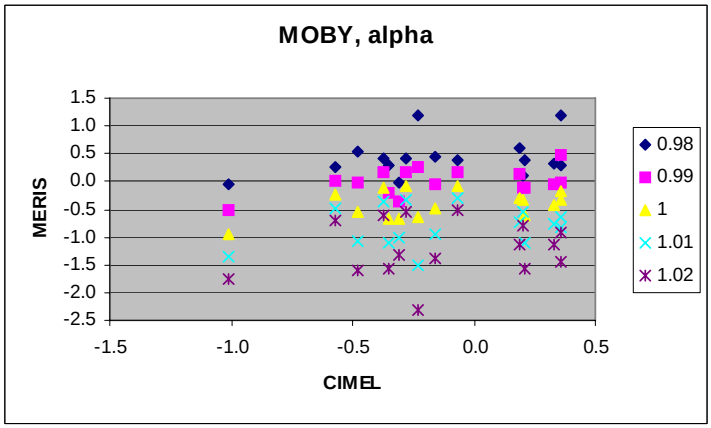

Figure 17: same as figure 15 but with threshold on the AOT_865

4.1.2 Absolute calibration of MERIS using ε

Figure 18 gives the relative contribution of the mixing layer to the TOA signal. For high meteorological visibilities, the contribution of the mixing layer is relatively small compares to the molecular one. Despite this favorable condition (rely on the well known Rayleigh scattering), an absolute calibration within few percent is difficult to achieve: complementary to the AOT, the aerosol phase needs to be know accurately. The reference to standard aerosol models can not result in accurate estimates of the phase function. The use of the CIMEL sky radiances to predict the phase function is an option (Martiny et al, 2005 a & b) which needs first to be carefully implemented and second to be processed on a significant number of calibration days.

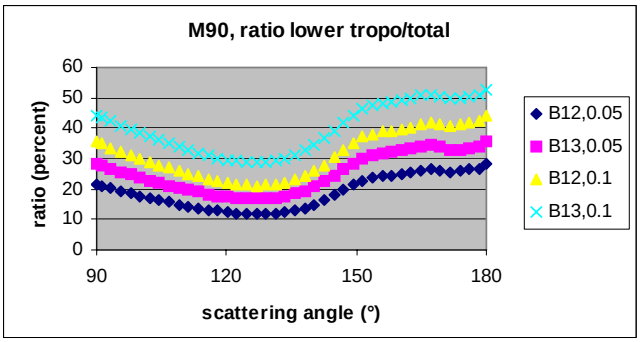

Figure 18: the relative contribution of ro_aer for the mixing layer is reported versus the scattering angle in B12 and B13 for two values of the AOT_550: 0.05 and 0.1 of this layer.

The sensitivity of ε to the radiometric calibration is high as illustrates in figure 19 for the maritime model. The sensitivity is reduced going towards the forward scattering because the aerosol reflectance dominates the Rayleigh one. The situation is less favorable in backscattering also because the aerosol backscattering increases more that the Rayleigh component.

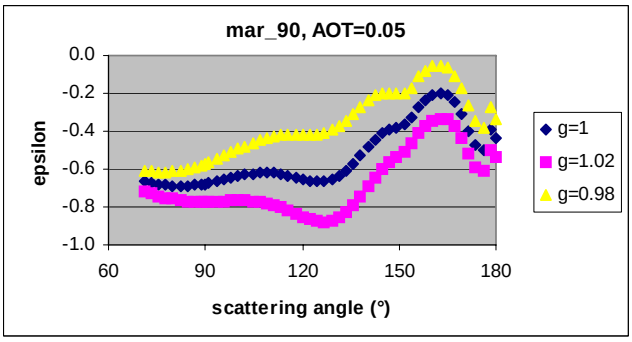

(a)

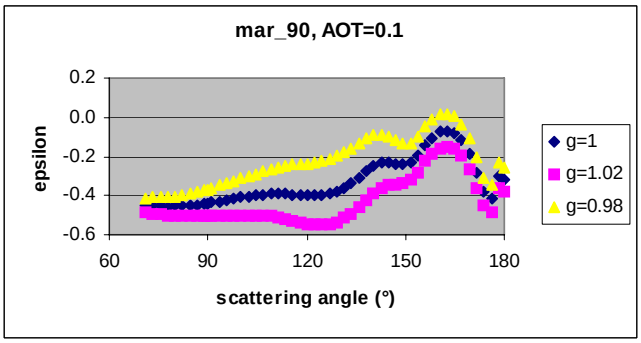

(b)

Figure 19: Sensitivity of ε to the radiometric calibration for 3 corrective factors g. The aerosols in the lower troposphere correspond to the maritime 90 model with an AOT_865 respectively equal to 0.005 (a) and 0.1 (b).

At a first order, in the primary scattering approximation, we get:

$$\varepsilon = \ln(\tau_a^{\lambda} P_a^{\lambda}(\Theta) / \tau_a^{\lambda'} P_a^{\lambda'}\Theta)) / \log(\lambda / \lambda') \qquad (12)$$

Actually, $P_a^{\lambda}(\Theta)$ is the aerosol phase function time the single scattering albedo. We can compare ε from up (MERIS) and from down (CIMEL) if the measurements are made at the same scattering angle following the geometrical conditions illustrate in figure 18.

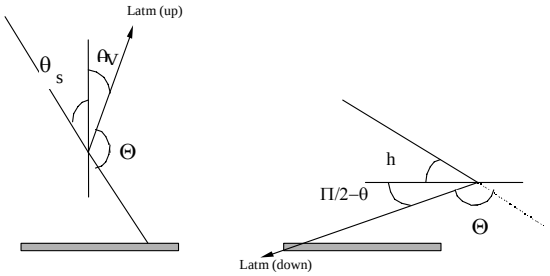

Figure 20: geometrical correspondence at the same scattering angle between ground-based and satellite measurements.

This correspondence on the atmospheric path radiance between satellite and ground based measurements is not easy to achieve:

(i) The maximum scattering angle Θ reaches from the ground is 150°. This angle correspond to solar zenith angle of about 75°. Eq. (12) certainly needs to be refined to account for the multiple scattering.

(ii) The simultaneity at same Θ between satellite and ground based measurements is very occasional. On an operational point of view, it is required to have on different AERONET sites an automatic process of AERONET and satellite data acquisition. The small differences in time are acceptable on clear stable days, a condition to be assessed.

(iii) At the end, the radiometric calibration of the CIMEL instrument should be better accurate than the requirement we have for the satellite sensor. CIMEL in AERONET is calibrated in laboratory on an integrated sphere within 2 percent errors. Therefore, it is certainly necessary to implement in situ calibration protocols. For low aerosol loading, a Rayleigh based calibration even in the NIR is an option (Santer et al, 2008).

4.3 The spectral dependence of the aerosol reflectance

The question is how to make compatible figure 4 and figure 7, what we measured and what we expect? We first applied the same radiometric calibration adjustment on B9, B12 and B13. For 5 multiplicative factors on the TOA reflectance, we ratio the aerosol reflectance in B13 to the predicted value by ln-ln extrapolation from B9-B12 to B13. The results, figure 21 suggest that the 3 percent bias in figure 4 can be not recovered by a white shift of the radiometric calibration. It is quite insensitive to this adjustment.

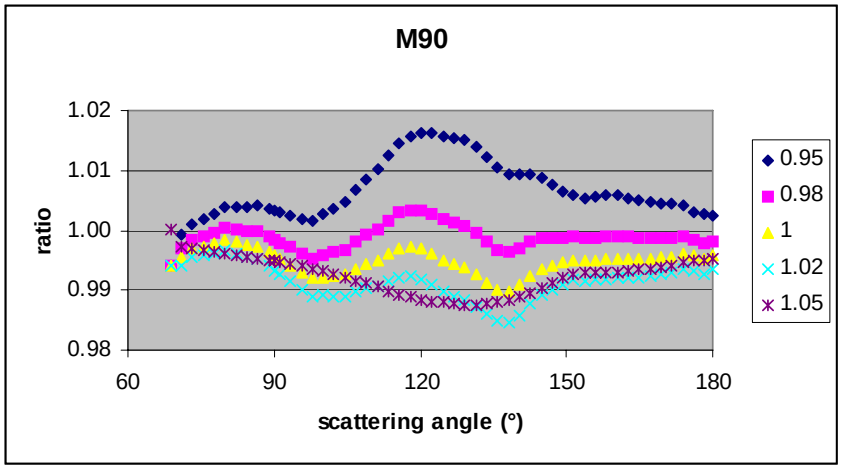

Figure 21: Ratio of the predicted to the exact aerosol reflectance in B13 for the M90 model and an AOT_550=0.1. This ratio is given for five values of the calibration adjustment: 0.95, 0.98,1, 1.02, 1.05.

We then considered an inter band calibration with the major weight in B13 and no change in B9. We apply relative corrections in B13 of 0.95, 0.98, 1, 1.02 and 1.05 and in B12 of 0.975, 0.99, 1, 1.01 and 1.025. Results in figure 22 for M90 suggest that a gain of around 0.97 at 865 nm.

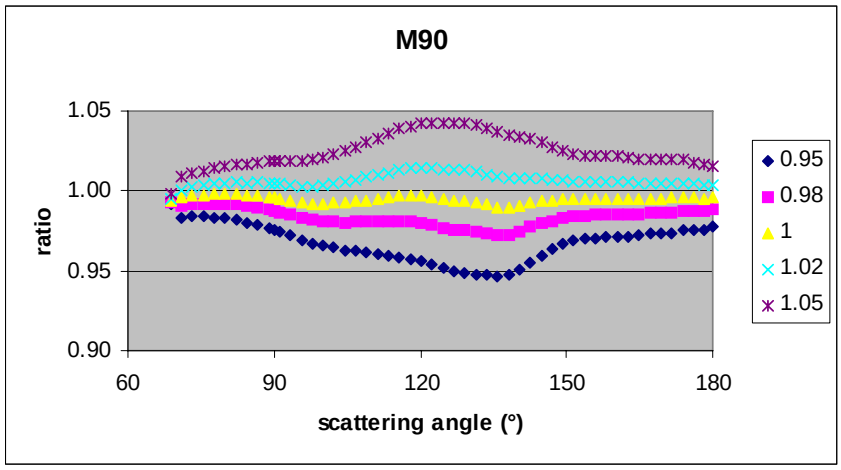

Figure 22: Ratio of the predicted to the exact aerosol reflectance in B13 for the M90 model and an AOT_550=0.1. This ratio is given for five values of the inter band calibration adjustment at 708 nm (see text): 0.95, 0.98,1, 1.02, 1.05.

The spectral alignment of the aerosol reflectance depends on the knowledge of the instrument behaviour. If only 865 nm is questionable, then the following adjustment is conducted:

(i) on oligotrophic waters

(ii) on a prediction of the aerosol reflectance in B13 from the ln-ln spectral extrapolation from B9 and B12.

(iii) On a recomposition of the TOA reflectance in B13 and a comparison to it measurements.

This method should be applied on a statistical basis, with a research of the trends versus the relevant geophysical parameters: level of TOA signal, scattering angle,…

4.4 A better retrieval of the aerosol optical thickness

4.4.1 Use the IOPA models

Regarding the continuity of the aerosol IOPs versus α (or ε), we already pointed out the advantage of using the IOPA models (§4.1.2). The same recommendation applies for the vertical distribution (§4.1.3).

In addition, the IOPA models reflects directly the optical properties of the aerosols.

4.4.2 Characterize the aerosols in the backscattering

The poor comparison on the AOT between MERIS and CIMEL in MOBY mostly results from the poor knowledge of the aerosol phase function P_a in the back scattering.

Multi view sensors (POLDER, MIRS, AATSR) offers the potentiality to better evaluate P_a in the backscattering. If we rely on outside off the backscattering, we get the AOT. Reciprocally, in the backscattering, starting from the AOT, we can retrieve P_a.

Based on simultaneous MERIS and CIMEL acquisitions, the possible strategy is the following:

(i) AOT's from CIMEL will allow selecting a SAM as associate $P_{SAM}(\Theta)$

(ii) The SO code will be used to predict the MERIS TOA radiances at 708 *nm*, 778 *nm* and 870 *nm*.

(*iii*) This reference computation will allows defining the factor g as follows:

$$L_{sim} = g \cdot \tau_{cimel} \cdot P_{SAM}(\Theta) \quad (13)$$

(*iv*) If g is not sensitive to the aerosol model, then we will derive the APF from the MERIS observations (P_{MERIS}) as:

$$(L_{MERIS} - L_{sim}) / L_{sim} = \tau_{cimel} (P_{MERIS} - P_{SAM}) / P_{SAM} \quad (14)$$

ACKNOWLEDGEMENTS

The authors would like specially to thank all the PI's in the use of the different CIMEL instruments from AERONET.

Commentaire [s1] : Remercier celui de Lampedusa

REFERENCES

Antoine, D., and A. Morel, 1999. A multiple scattering algorithm for atmospheric correction of remotely sensed ocean color (MERIS instrument): principle and implementation for atmospheres carrying various aerosols including absorbing ones, *International Journal of Remote Sensing*, 20 (9): 1875-1916.

Delwart S., L. Bourg and J.P. Huot, 2003, MERIS 1st year: Early calibration results, *Proceedings of the International Society for Optical Engineering (SPIE): Sensors, Systems and Next-Generation Satellite VII, Barcelona, Spain.* Vol. 5234, pp. 379–390.

Delwart S., Preuker R., Bourg L., Santer R., Ramon D., Fischer J., 2007 MERIS In-flight Spectral Calibration. International Journal of Remote Sensing. Vol 28.

Cox, C., and W. Munk, 1954. Measurements of roughness of the sea surface from photographs of the sun glitter, *Journal of Optical Society in America*, 44 (11): 838-888.

Deuzé, J.L., M. Herman, and R. Santer, 1989. Fourier series expansion of the transfer equation in the atmosphere-ocean system, *Journal of Quantitative Spectroscopy & Radiative Transfer*, 41 (6): 483-494.

Franz B. A., Sean W. Bailey, P. Jeremy Werdell and Charles R. McClain, Sensor-independent approach to vicarious calibration of satellite ocean color radiometry, Applied Optics 46, 5068—5082 (2007).

Gordon H. R., and M. Wang, "Retrieval of water-leaving radiances and aerosol optical thickness over the oceans with SeaWiFS : a preliminary algorithm", *Appl. Opt*., Vol. 33, No. 3, 443-452, 1994

Holben, B., T. Eck, I. Slutsker, D. Tanré, J.P. Buis, A. Setzer, E. Vermote, J. Reagan, Y. Kaufman, T. Nakajima, F. Lavenu, I. Jankowiak, and A. Smirnov, 1998. AERONET – A federated instrument network and data archive for aerosol characterization, *Remote Sensing of Environment*, 66: 1-16.

Huot J.P.,2008. Consideration on the monotonicity with wavelength of the"aerosol" signal in the NIR. Personnal communication.

Lenoble J., M. Herman, J.L. Deuzé , B. Lafrance, R. Santer, D. Tanre, 2007. A successive order of scattering code for solving the vector equation of transfer in the earth's atmosphere with aerosols.Journal of Quantitative Spectroscopy &Radiative Transfer 107 (2007) 479–507.

Mazeran C., 2007. Quality Control methodology for validating Ocean Atmospheric Correction, Report, ACRI ST.

Martiny N., R Santer, and I. Smolskaia, 2005-a. Vicarious calibration of MERIS over dark waters in the near-infrared, *Journal of Remote Sensing and Environnement*, 94 (4): 475-490.

Martiny N., R. Frouin, and R. Santer, 2005-b. Vicarious calibration of SeaWiFS in the near-infrared using the dark ocean, *Applied Optics*.

Myhre G., Stordal F., Johnsrud M., Ignatov A., Mischenko M., Geogdzhayev I. V., Tanré D., Deuzé J.L., Goloub P., Nakajoma T., Higurashi A., Torres O. and Holben B. 2004. Intercomparison of Satellite Retrieved Aerosol Optical Depth over the Ocean ; *Journal of Atmospheric Sciences, Vol. 61.*

Nobileau, D. and D. Antoine (2005) Detection of blue-absorbing aerosols using near infrared and visible (ocean color) remote sensing observations. *Remote Sensing of Environment*, **95**, 368-387

Santer R., Carrere V., Dubuisson P., & Roger J.C. (1999). Atmospheric correction over land for MERIS, International Journal of Remote Sensing, Vol. 20. Issue 9, p 1819-1840.

Santer R., and N. Martiny, 2003. Sky radiance measurements for ocean colour calibration-validation, *Applied Optics*, 42 (6): 896-907.

Santer R., Meygret A., Buis J.P. , "Atmosphere and land optical characterization using automatic ground based measurements". Accepted for publication to International Journal of Remote Sensing, October 2008 ,

Schaepman M., Milla Z., Kneubueher M., Clevers J., Delwart S. , 2004, " Assessment of long-term vicarious calibration efforts of MERIS on land product quality". Sensors, Systems, and Next-Generation Satellites VIII. Edited by Meynart, Roland; Neeck, Steven P.; Shimoda, Haruhisa. Proceedings of the SPIE, Volume 5570, pp. 363-371.

Shettle, E.P., and R.W. Fenn, 1979. Models for the aerosols of the lower atmosphere and the effects of humidity variations on their optical properties, *Air Force Geophysical Laboratory*, *Technical Report AFGL-TR-79-0214*, Hanscom Air Force Base (Mass.).

Wang M. and H. R. Gordon, 2002. Calibration of ocean color scanners: how much error is acceptable in the near infrared? Remote Sens. Environ. 82, 497—504.

Zagolski, F., R. Santer, Aznay O., 2007, A new climatology for atmospheric correction based on the aerosol inherent optical properties**.** *Vol. 112, No. D14, D14208*